
Contents

Figures	page xi
Preface	xv
1 Introduction	1
1.1 The Schwarz–Christoffel idea	1
1.2 History	5
2 Essentials of Schwarz–Christoffel mapping	11
2.1 Polygons	11
2.2 The Schwarz–Christoffel formula	12
2.3 Polygons with one or two vertices	14
2.4 Triangles	19
2.5 Rectangles and elliptic functions	21
2.6 Crowding	23
3 Numerical methods	27
3.1 Side-length parameter problem	27
3.2 Quadrature	32
3.3 Inverting the map	34
3.4 Cross-ratio parameter problem	35

3.5	Mapping using cross-ratios	41
3.6	Software	45
4	Variations	47
4.1	Mapping from the disk	48
4.2	Mapping from a strip	49
4.3	Mapping from a rectangle	54
4.4	Exterior maps	60
4.5	Periodic regions and fractals	61
4.6	Reflections and other transformations	66
4.7	Riemann surfaces	67
4.8	Gearlike regions	69
4.9	Doubly connected regions	73
4.10	Circular-arc polygons	79
4.11	Curved boundaries	84
5	Applications	87
5.1	Why use Schwarz–Christoffel maps?	88
5.2	Piecewise-constant boundary conditions	89
5.3	Alternating Dirichlet and Neumann conditions	93
5.4	Oblique derivative boundary conditions	100
5.5	Generalized parameter problems	113
5.6	Free-streamline flows	115
5.7	Mesh generation	120
5.8	Polynomial approximation and matrix iterations	123
5.9	Symmetric multiply connected domains	127
	Using the SC Toolbox	131
	Bibliography	137
	Index	151

Figures

1.1	Notational conventions	2
1.2	Action of a term in the SC product	3
1.3	The effect of prevertices on side lengths	4
1.4	Schwarz's plot of the conformal map to a square	6
2.1	Interior angles for a vertex at infinity	12
2.2	Map from the disk to a half-plane	15
2.3	Map from the half-plane to a strip	16
2.4	Map from the disk to a strip	16
2.5	A different map of the half-plane to a strip	17
2.6	Map from a doubly slit plane using reflection	17
2.7	Other maps obtained by reflection	18
2.8	Maps from the half-plane to wedges	19
2.9	Maps to triangles with two infinite vertices	20
2.10	Maps to triangles with one infinite vertex	21
2.11	Map from the half-plane to a rectangle	22
2.12	Map from a generalized quadrilateral	23
2.13	Illustration of crowding	24
3.1	Location of the last vertex by intersection	29
3.2	Maps to regions with 100 vertices	31
3.3	Endless descent in the side-length parameter problem	31

3.4	Embeddings with different crowding localities	36
3.5	Triangulation and quadrilaterals in the CRDT scheme . .	38
3.6	Summary of the CRDT idea	40
3.7	Preprocessing step for CRDT	41
3.8	Map to a “maze” using CRDT	43
3.9	Map to the maze from a multiply elongated region	44
4.1	Examples of disk maps	50
4.2	More examples of disk maps	51
4.3	Elementary factor in the strip map	52
4.4	Divergence adjustment of the strip map	53
4.5	Examples of strip maps	55
4.6	More examples of strip maps	56
4.7	Comparing the rectangle, half-plane, and strip	57
4.8	Examples of rectangle maps	58
4.9	More examples of rectangle maps	59
4.10	Examples of exterior maps	62
4.11	More examples of exterior maps	63
4.12	Map to a periodic channel	64
4.13	Map to a self-similar spiral.	65
4.14	Map to a symmetric doubly connected region by reflection	66
4.15	Map to a symmetrically periodic channel by reflection . .	67
4.16	Maps to certain regions with circular arcs	68
4.17	Map to a three-sheeted Riemann surface	70
4.18	Maps to gearlike regions	71
4.19	Logarithms of the gearlike regions	72
4.20	Notation for the doubly connected map	73
4.21	First steps toward the doubly connected map	75
4.22	Convergence of a doubly connected SC factor	76
4.23	Examples of doubly connected SC maps	80
4.24	Maps to circular-arc polygons	83
5.1	Solving Laplace’s equation with two boundary values . .	90
5.2	Components of a piecewise-constant harmonic function .	92
5.3	Examples of four-boundary-value harmonic functions . .	94
5.4	More piecewise-constant Dirichlet examples	95
5.5	Solutions to the D/N/D/N Laplace problem	97
5.6	Solutions of three-value alternating D/N problems . . .	97
5.7	Riemann surface in the four-value alternating D/N prob- lem	100

5.8	Examples of alternating D/N solutions	101
5.9	More examples of alternating D/N solutions	102
5.10	Oblique derivative problem on an L-shaped region . . .	104
5.11	Solution of the L-shaped oblique derivative problem . . .	104
5.12	More solutions to the L-shaped oblique problem	105
5.13	Examples from a space of solutions to an oblique deriva- tive problem	109
5.14	More examples of solutions to oblique derivative problems	110
5.15	Illustration of the Hall effect	111
5.16	Illustration of reflected Brownian motion	112
5.17	Resistor trimming problem	114
5.18	Multiple resistance measurements for locating cracks . .	115
5.19	Wake flow past a polygonal obstacle	116
5.20	Potential and computational planes for wake flow	117
5.21	Elementary factor in the free-streamline map	118
5.22	Examples of wake flows	121
5.23	Notation for approximation discussion	124
5.24	Level curves of Faber polynomials	126
5.25	Green's function for a symmetric multiply connected re- gion	128
5.26	More examples of Green's functions	130

Preface

In the autumn of 1978, Peter Henrici took leave from the ETH in Zurich to visit the Numerical Analysis Group at Stanford University. The second author, then a graduate student, asked Henrici if he might propose a project in the area of computational complex analysis. Henrici's suggestion was, why don't you see what you can do with the Schwarz–Christoffel transformation?

For months thereafter LNT spent all of every weekend working on SC mapping at the computer terminals of the Stanford Linear Accelerator Center. This brief but intense project led to one of the first technical reports ever printed in \TeX , which was published in the first issue of the *SIAM Journal on Scientific and Statistical Computing*; to the FORTRAN package SCPACK; and to a lasting love of numerical conformal mapping. In the following years it led further to extensions and applications of SC ideas carried out in collaboration with various people, including Alan Elcrat and Frédéric Dias on free-streamline flows, Ruth Williams on oblique derivative problems, and Louis Howell on modified formulas for elongated regions.

By the early 1990s, LNT was a faculty member at Cornell University and the first author was a graduate student. We worked together on a number of topics from hydrodynamic stability to “Can one hear the shape of a drum?”, but the subject we kept coming back to was

Schwarz–Christoffel mapping. Once again it started with a brief suggestion. MATLAB graphics had become widespread, and LNT proposed to TAD, why not convert SCPACK to an interactive MATLAB package? The resulting SC Toolbox was even more fun than we had imagined. We quickly became accustomed to drawing a polygon with a mouse, clicking a button, and seeing in seconds a plot of a conformal map correct to eight digits. The SC Toolbox was one of the earliest advanced applications built around a MATLAB graphical user interface. It matured as MATLAB did, quickly eclipsing SCPACK by surpassing it not just in convenience but also in capabilities and numerical power. (The second author insists on adding that a parallel development occurred as TAD quickly overtook LNT in his knowledge of Schwarz–Christoffel mapping.)

Mathematically, the subject continued to grow. Others such as Henrici (before his death in 1986), Däppen, and Floryan and Zemach had made important contributions. A new collaborator was Steve Vavasis, who together with TAD developed the CRDT algorithm. Based on Delaunay triangulation and Möbius transformations, it is very different from other methods in concept and is largely immune to the problems of exponential crowding. Applications to large-scale nonsymmetric matrix iterations were pursued in collaboration with Kim-Chuan Toh. Applications to the computation of Green’s functions and their uses in approximation theory and digital filtering were developed with Mark Embree. We came to realize that although experts in complex analysis had a depth of theoretical understanding that we could not match, we had accumulated an experience of the practical side of SC problems and of the range of their variations and applications that was unique.

The result is this book. Our style is concise, covering more material than might be expected in the small number of pages. For nearly every topic we have included a number of computer-generated figures, all of which are not just schematic but quantitatively correct. We hope that these figures will quickly tell the reader *what* one can do with these methods—always with high speed and accuracy—and that careful reading if desired will reveal the details of *how*. To assist in this latter purpose, an appendix gives short MATLAB scripts showing how to generate some of our figures with the help of the SC Toolbox.

We thank those whose comments and contributions improved this book. Endre Süli and Markus Melenk helped us link the one-half quad-

rature rule with mesh refinement in finite elements; Lehel Banjai conducted experiments regarding the refinement ratio. Tom DeLillo, Alan Elcrat, and John Pfaltzgraff shared an advance copy of their work on doubly connected maps and thereby sparked our discussion in section 4.9. Louis Howell generously created the data for the circular-arc mappings in Figure 4.24. Martin Gutknecht and Dieter Gaier shared many discussions on conformal mapping with the second author over the years. For inspiration, we are grateful to Peter Henrici, who in many ways is the person most responsible for this book.

CHAPTER 1

Introduction

1.1 The Schwarz–Christoffel idea

The idea behind the Schwarz–Christoffel (SC) transformation and its variations is that a conformal transformation f may have a derivative that can be expressed as

$$f' = \prod f_k \tag{1.1}$$

for certain canonical functions f_k . A surprising variety of conformal maps can be fit into this basic framework. In fact, virtually all conformal transformations whose analytic forms are known are Schwarz–Christoffel maps, albeit sometimes disguised by an additional change of variables.

Geometrically speaking, the significance of (1.1) is that

$$\arg f' = \sum \arg f_k.$$

In the classical transformation, each $\arg f_k$ is designed to be a step function, so the resulting $\arg f'$ is piecewise constant with specific jumps —i.e., f maps the real axis onto a polygon. To be specific, let P be the region in the complex plane \mathbf{C} bounded by a polygon with ver-

plicitly.

In the majority of practical problems, there is no analytic solution for the prevertices, which depend nonlinearly on the side lengths of Δ . Numerical computation is also usually needed to evaluate the integral in (1.4) and to invert the map. Thus, much of the potential of SC mapping went unrealized until computers became readily available in the last quarter of the twentieth century. Numerical issues are discussed in Chapter 3.

1.2 History

The roots of conformal mapping lie early in the nineteenth century. Gauss considered such problems in the 1820s. The Riemann mapping theorem was first stated in Riemann's celebrated doctoral dissertation of 1851: Any simply connected region in the complex plane can be conformally mapped onto any other, provided that neither is the entire plane.³ The Schwarz–Christoffel formula was discovered soon afterward, independently by Christoffel in 1867 and Schwarz in 1869.

Elwin Bruno Christoffel (1829–1900) was born in the German town of Montjoie (now Monschau) and was studying mathematics in Berlin under Dirichlet and others when Riemann's dissertation appeared.⁴ Christoffel completed his doctoral degree in 1856 and in 1862 succeeded Dedekind as a professor of mathematics at the Swiss Federal Institute of Technology in Zurich. It was in Zurich that he published the first paper on the Schwarz–Christoffel formula, with the Italian title, “Sul problema delle temperature stazionarie e la rappresentazione di una data superficie” [Chr67]. Christoffel's motivation was the problem of heat conduction, which he approached by means of the Green's function. This paper presented the discovery that, in the case of a polygonal domain, the Green's function could be obtained via a conformal map from the half-plane, as in (1.4). In subsequent papers he extended these ideas to exteriors of polygons and to curved boundaries [Chr70a, Chr70b, Chr71].

³ Riemann's proof, based on the Dirichlet principle, was later pointed out by Weierstrass to be incomplete. Rigorous proofs did not appear until the work of Koebe, Osgood, Carathéodory and Hilbert early in the twentieth century.

⁴ For extensive biographical information on Christoffel, the reader is referred to the sesquicentennial volume [BF81], particularly Pfluger's paper therein on Christoffel's work on the SC formula.

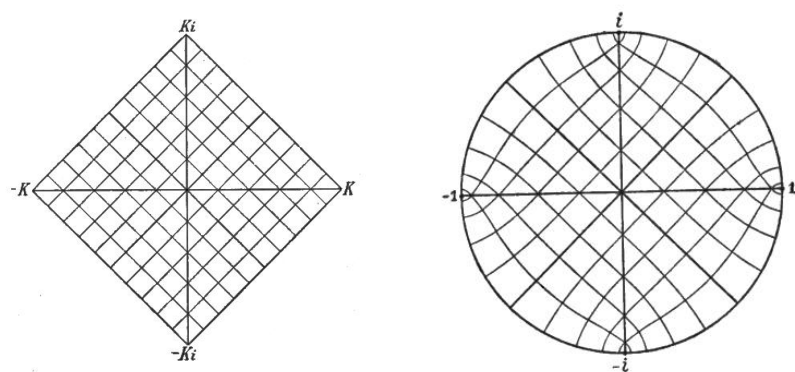


Figure 1.4. Schwarz's 1869 plot of the conformal map from a square onto a disk, reproduced from [Sch69b].

Hermann Amandus Schwarz (1843–1921) grew up nearly a generation after Christoffel but also very much under the influence of Riemann. In the late 1860s he was living in Halle, where his discovery of the Schwarz–Christoffel formula apparently came independently of Christoffel's. His three papers on the subject [Sch69a, Sch69b, Sch90] cover much of the same territory as Christoffel's, including the generalizations to curved boundaries (section 4.11) and to circular polygons (section 4.10), but the emphasis is quite different—more numerical and more concerned with particular cases such as triangles in [Sch69b] and quadrilaterals in [Sch69a].⁵ Schwarz even published the world's first plot of a Schwarz–Christoffel map, reproduced in Figure 1.4. Schwarz's papers included his famous reflection principle: if an analytic function f , extended continuously to a straight or circular boundary arc, maps the boundary arc to another straight or circular arc, then f can be analytically continued across the arc by reflection.

In 1869 Christoffel moved briefly to the Gewerbeakademie in Berlin, and Schwarz succeeded him in Zurich. By this time, the two were well aware of each other's work; the phrase *Schwarz–Christoffel transformation* is now nearly universal (although the order of the names is reversed in some of the literature of the former Soviet Union).

In the 130 years since its discovery, the Schwarz–Christoffel formula

⁵ Schwarz also credits Weierstrass for proving the existence of a solution for the unknown parameters (which Schwarz proved for $n = 4$) in the general case.

- Beigel** (1969)
Hoffman (1971, 1974)
Gaier [Gai72]: “Crowding” phenomenon
Howe [How73]
Vecheslavov, Tolstobrova & Kokoulin [VT73, VK74]: Doubly connected regions
Foster & Anderson [FA74, And75]
Cherednichenko & Zhelankina [CZ75]
Squire [Squ75]
Meyer [Mey79]: Comparison of algorithms
Nicolaide [Nic77]
Prochazka [HP78, Pro83]: FORTRAN package KABBAY
Davis et al. [Dav79, ADHE82, SD85]: Curved boundaries
Hopkins & Roberts [HR79]: Solution by Kufarev’s method
Reppe [Rep79]: First fully robust algorithm
Binns, Rees & Kahan [BRK79]
Volkov [Vol79, Vol87, Vol88]
Trefethen [Tre80, Tre84, Tre89, Tre93]: Robust algorithm, SCPACK, generalized parameter problems
Brown [Bro81]
Tozoni [Toz83]
Hoekstra (1983, [Hoe86]): Curved boundaries, doubly connected regions
Sridhar & Davis [SD85]: Strip maps
Floryan & Zemach [Flo85, Flo86, FZ87]: Channel flows, periodic regions
Bjørstad & Grosse [BG87]: Software for circular-arc polygons
Dias, Elcrat & Trefethen [ET86, DET87, DE92]: Free-streamline flows
Däppen [Däp87, Däp88]: Doubly connected regions
Costamagna ([Cos87, Cos01]): Applications in electricity and magnetism
Howell & Trefethen [How90, HT90, How93, How94]: Integration methods, elongated regions, circular-arc polygons
Pearce [Pea91]: Gearlike domains
Chaudhry [Cha92, CS92]: Piecewise smooth boundaries
Gutlyanskii & Zaidan [GZ94]: Kufarev’s method
Driscoll [Dri96]: SC Toolbox for MATLAB
Hu [Hu95, Hu98]: Doubly connected regions (FORTRAN package DSCPACK)

CHAPTER 2

Essentials of Schwarz–Christoffel mapping

2.1 Polygons

For the rest of this book, a (generalized) **polygon** is defined by a collection of vertices w_1, \dots, w_n and real interior angles $\alpha_1\pi, \dots, \alpha_n\pi$. It is convenient for indexing purposes to define $w_{n+1} = w_1$ and $w_0 = w_n$. The vertices, which lie in the extended complex plane $\mathbb{C} \cup \{\infty\}$, are given in counterclockwise order with respect to the interior of the polygon (i.e., locally the polygon is “to the left” as one traverses the side from w_k to w_{k+1}).

The interior angle at vertex k is defined as the angle swept from the outgoing side at w_k to the incoming side. If $|w_k| < \infty$, we have $\alpha_k \in (0, 2]$. If $\alpha_k = 2$, the sides incident on w_k are collinear, and w_k is the tip of a slit. The definition of the interior angle is applied on the Riemann sphere if $w_k = \infty$. In this case, $\alpha_k \in [-2, 0]$. See Figure 2.1. Specifying α_k is redundant if w_k and its neighbors are finite, but otherwise α_k is needed to determine the polygon uniquely.

In addition to the preceding restrictions on the angles α_k , we require

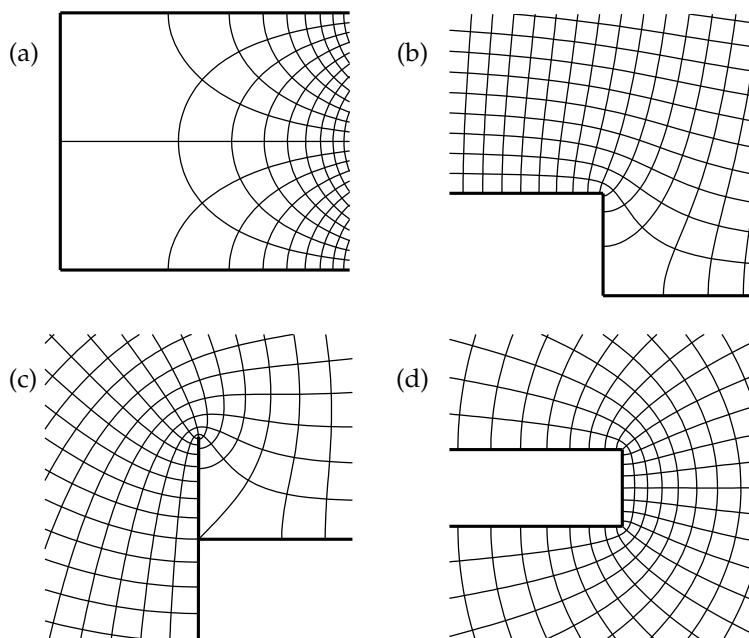


Figure 2.10. Maps from the half-plane to triangles with one infinite vertex. The curves are images of regular cartesian grids. The letters refer to formulas (2.10a)–(2.10d).

2.5 Rectangles and elliptic functions

If $n = 4$, the Schwarz–Christoffel prevertices are not ours to choose. In the general case there is no simple analytic determination of the one degree of freedom in the prevertices. However, in the important case when P is the interior of a rectangle, symmetry allows an explicit solution.

We rotate and translate the rectangle so that its vertices are $w_1 = K + iK'$, $w_2 = -K$, $w_3 = K$, and $w_4 = K + iK'$. (The motivation for the notation will become clear shortly.) By symmetry, we choose the prevertices as $z_1 = -m^{1/2}$, $z_2 = -1$, $z_3 = 1$, and $z_4 = m^{1/2}$, where m is a parameter that represents the degree of freedom in the prevertices. The image of infinity turns out to be the point iK' , and the image of 0 is 0. See Figure 2.11. The mapping function can be written as an elliptic

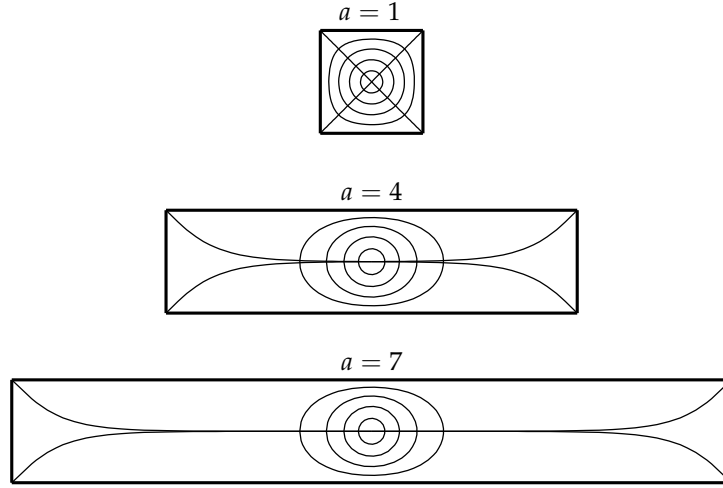


Figure 2.13. Illustration of the “crowding” phenomenon in maps of the disk to rectangles of different aspect ratio a . The angles subtended at the origin are $\pi/2$, 0.00475, and 0.0000427.

small. This effect can be analyzed via the expansions

$$K = \frac{\pi}{2} + O(m),$$

$$K' = \log \frac{4}{m^{1/2}} + O(m \log m).$$

The aspect ratio a thus satisfies

$$a = \frac{K'}{2K} = \frac{1}{2\pi} \log \frac{16}{m} + O(m \log m),$$

$$m = O(e^{-2\pi a}). \quad (2.12)$$

The cross-ratio (see p. 36) of the four prevertices $m^{-1/2}, -1, 1, m^{-1/2}$ is therefore $O(m^{1/2}) = O(e^{-\pi a})$. Since any map of the upper half-plane to the disk preserves this cross-ratio, some pair of prevertices in any disk map to the rectangle of aspect ratio a will be separated by a distance that is $O(e^{-\pi a/2})$.

In the vicinity of those crowded prevertices, the derivative of the map $f(z)$ must be $O(e^{\pi a/2})$. This indicates that tiny changes in a point in

CHAPTER 3

Numerical methods

Methods for the numerical computation of Schwarz–Christoffel maps have been refined for 40 years, and improvements continue. At this writing, it is possible to compute (to, say, eight accurate digits) maps to regions with one or two dozen vertices in a few seconds on a workstation. Regions with a hundred vertices can be treated in a few minutes.

In this chapter we shall examine the major algorithmic issues of SC mapping and refer to the literature for the full numerical analysis. For concreteness we describe maps from the disk, which is often most convenient computationally; the half-plane is little different. The chapter closes with brief descriptions of relevant software packages available for free in the public domain.

3.1 Side-length parameter problem

At the heart of any numerical method for Schwarz–Christoffel maps is the solution of the parameter problem. The most successful general-purpose methodology, based on equations derived from side lengths, was introduced in 1980 by Trefethen [Tre80], who built on work by Reppe [Rep79] and others. Variations on this technique remain the

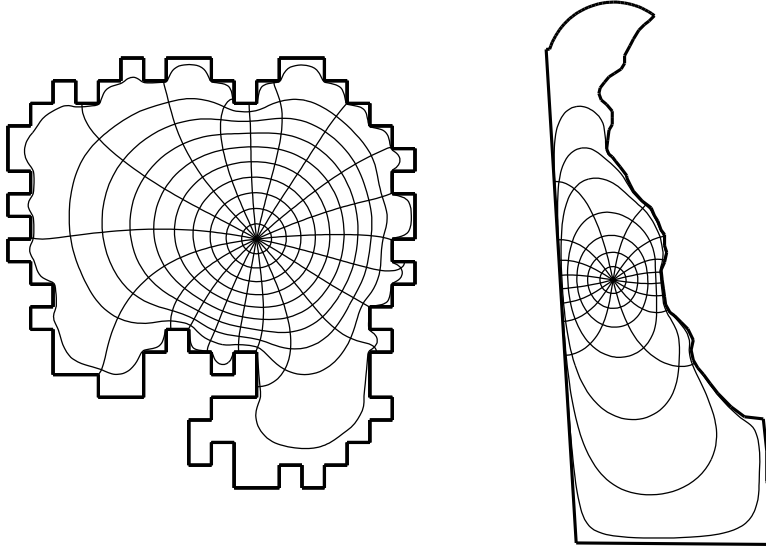


Figure 3.2. Maps to two regions with 100 vertices. The circular arc at the top of the state of Delaware (right) is approximated by 36 straight-line segments. In practice we recommend instead methods designed for smooth arcs.

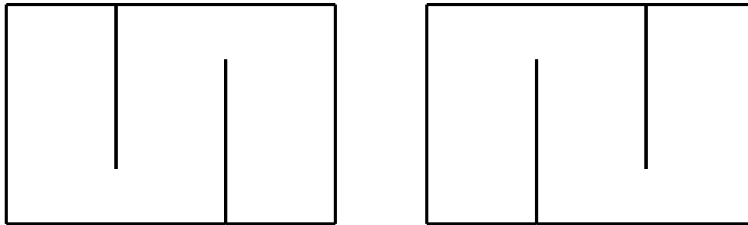


Figure 3.3. A descent method for the side-length parameter problem can never achieve the polygon on the right when starting from the polygon on the left.

Therefore, a descent method starting from an initial prevertex arrangement that maps to the region on the left will not converge to the region on the right—some sort of global “leap” is needed to allow the slits to cross. In practice, a breakdown like this is extremely rare, but regions

which is impossible [How90].

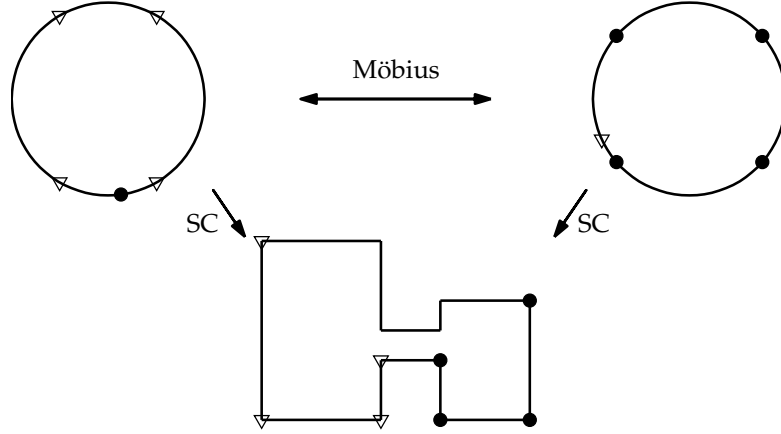


Figure 3.4. Both embeddings of the disk (top) map to the same polygon (bottom), but different groups of prevertices (dots and triangles) are clustered on the circle. Hence each version of the map is crowded in a different part of the polygon.

originates from fixing the three free parameters. A particular embedding is implicitly chosen at the start, and it must suffer from crowding somewhere. To circumvent crowding, we need a robust way to find the *family* of equivalent embeddings. More specifically, we need

1. A compact representation of the family, and
2. Access to locally well-conditioned embeddings from the family.

We begin with the first item. Any representation of an embedding family should have $n - 3$ real components. Moreover, because each embedding is related to any member of its family by a conformal map of the disk to itself (Möbius transformation), the family representation must be invariant under such maps. A good choice for the representation is to define $n - 3$ ordered 4-tuples of prevertices and take the **cross-ratio** of each, defined as [Neh52]

$$\rho(a, b, c, d) = \frac{(d - a)(b - c)}{(c - d)(a - b)}. \quad (3.5)$$

It is easily seen that for four points in counterclockwise order on the unit circle (or, in fact, any circle), the cross-ratio is real and negative. Cross-ratios are also invariant under Möbius transformations.

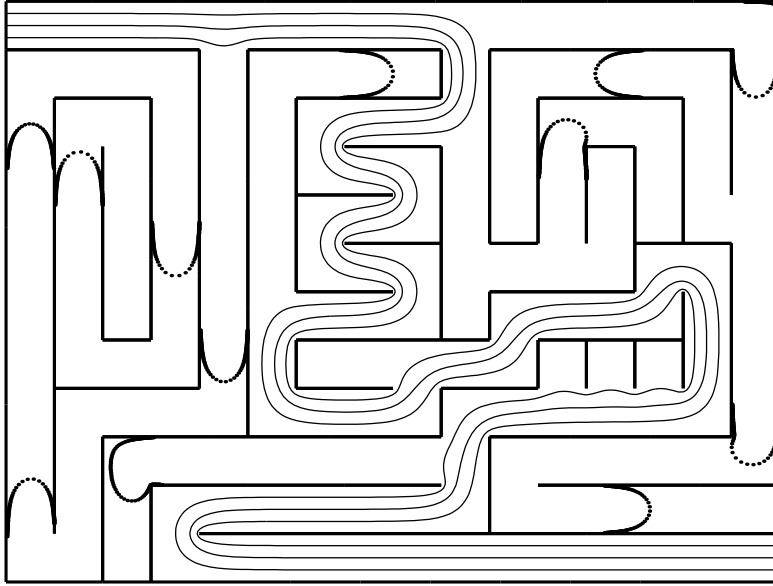


Figure 3.8. Map to a “maze” using the CRDT cross-ratio formulation. Each curve is the image of a line in a conformally equivalent rectangle; the dotted curves represent lines that are exponentially close ($10^{-10}, 10^{-20}, \dots, 10^{-50}$) to a rectangle side. All computations were done using double-precision arithmetic.

Another sort of map to the same region is illustrated in Figure 3.9. Instead of using the disk as an intermediary to a rectangle, the canonical region is multiply elongated to better match the “arms” of the maze. All the angles of this domain are multiples of $\pi/2$, which makes it simple to construct an orthogonal grid. The side lengths in this domain are not known a priori but must be found as part of the computation by evaluation of the SC integral; this is a generalization of the conformal modulus problem.

took about 10 lines of MATLAB code plus some human intervention.

3.6 Software

The most comprehensive and user-friendly numerical SC software is the Schwarz–Christoffel Toolbox for MATLAB. For more on the toolbox, how to obtain it, and examples of its use, see the appendix. Except where explicitly noted, all the examples and figures in this book were computed using this toolbox. (Some require a fair amount of programming in addition to the distributed toolbox code, however.)

The SC Toolbox is a descendent of SCPACK, a FORTRAN 77 package written by Trefethen [Tre80, Tre89]. SCPACK was responsible for first making numerical SC mapping widely available to nonexperts and has been in use for twenty years. Only maps from the disk, using the side-length formulation of the parameter problem, are directly supported; routines are included for computing the forward and inverse maps. SCPACK is available through the Netlib repository at <http://www.netlib.org/conformal>.

Also at Netlib in FORTRAN are:

DSCPACK A package written by Hu [Hu95] for mapping from annuli to doubly connected regions bounded by polygons (see section 4.9).

As in SCPACK, solving the parameter problem and computing maps in either direction are supported.

CAP A package by Bjørstad and Grosse [BG87] for mapping to circular-arc polygons (see section 4.10). This package is described by the authors as “experimental” and is not as robust as others listed here.

GEARLIKE A package written by Pearce [Pea91] for maps to “gear-like” domains (see section 4.8). It is modeled after SCPACK.

Finally, we mention three other public-domain packages for non-SC-based conformal mapping:

CONFPACK A FORTRAN package by Hough [HP83, Hou90] that implements Symm’s equation for simply connected regions (interior or exterior) with piecewise smooth boundaries. CONFPACK explicitly accounts for corner singularities [Hou89] and is very accurate and efficient. It is available at Netlib.

zipper A C package written by Marshall that implements an interpolation-based method of Kühnau [Küh83] for interior and exterior regions. Although corners are not explicitly accounted for, the software is remarkably fast. It is available from its author at <http://>

CHAPTER 4

Variations

A key aspect of the power of the Schwarz–Christoffel transformation (indeed, a large part of the motivation for this book) is its remarkable flexibility in adapting to a wide variety of situations, not all of which superficially seem to involve conformal maps or even polygons. The essence of SC mapping is to treat the corners exactly; if the rest of the problem is simple, nothing else is needed. What emerges from applications of this principle is that Schwarz–Christoffel mapping is not just a mapping technique but a unique way of thinking about problems of potential theory in the plane.

Let us reconsider the fundamental SC philosophy for constructing a map $f(z)$. For the half-plane, we required f' to have piecewise constant argument along the boundary, because then the image under f has straight lines with corners. For other canonical domains, we need to modify this requirement slightly. For example, as we follow the boundary of the unit disk, a constant argument for f' does not lead to a straight-line image. However, if $g(z)$ is a function that “straightens out” the original domain boundary, then f'/g' will have the appropriate piecewise-constant argument. This fact is especially convenient because we can also use powers of $g(z) - g(z_k)$ to create wedges that

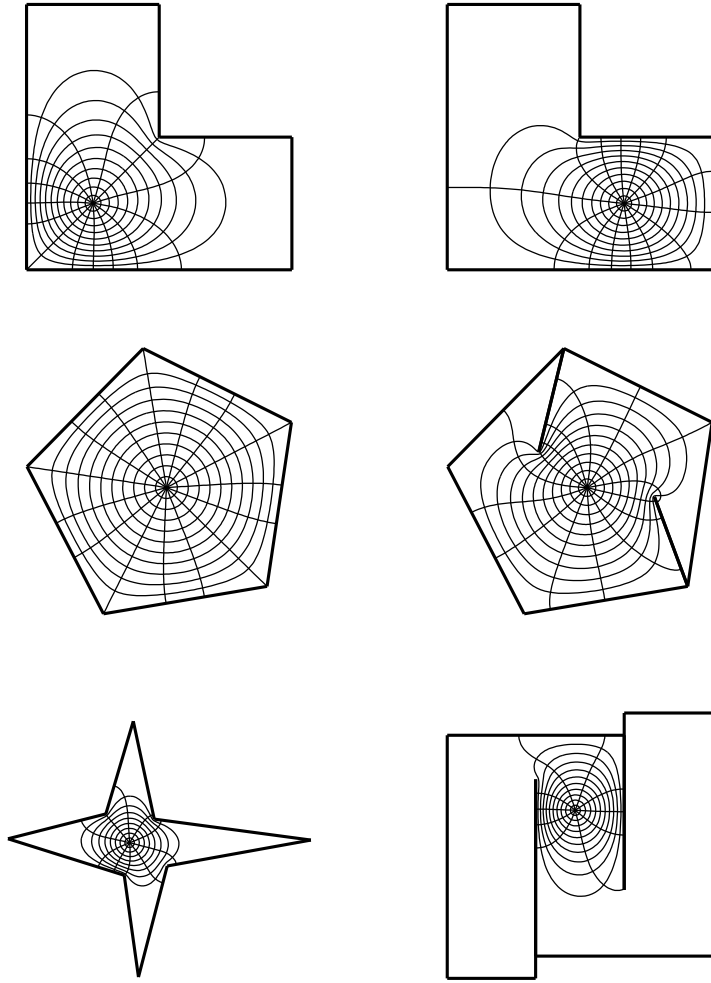


Figure 4.1. Examples of disk maps to bounded regions. In each case a regular polar grid in the disk is mapped to the target region. At bottom right, the pre-vertices on the unit circle are moderately crowded—their minimum separation is about 3.6×10^{-5} .

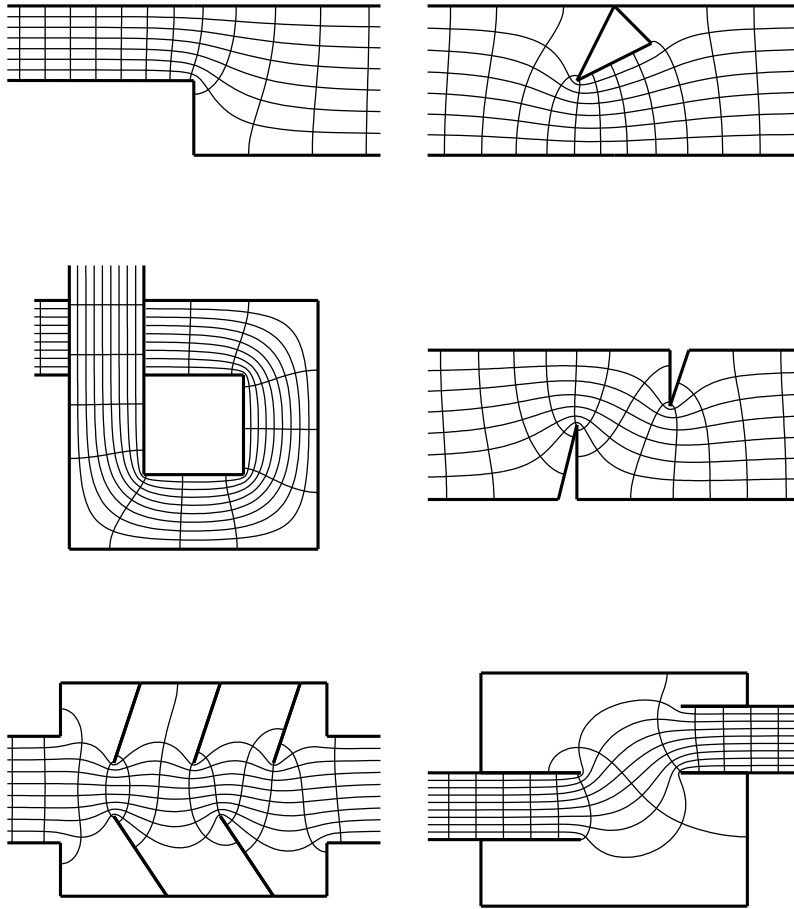


Figure 4.5. Examples of strip maps. In each case a regular cartesian grid in the infinite strip is mapped to the target region.

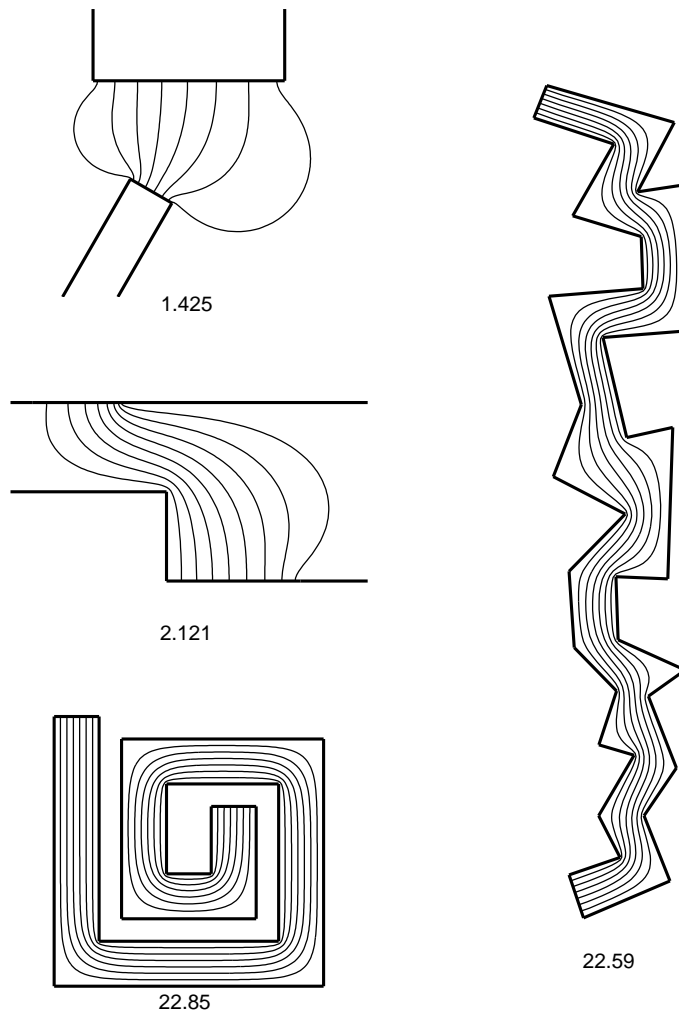


Figure 4.9. More examples of rectangle maps. Only one set of parallel lines from the rectangle is mapped.

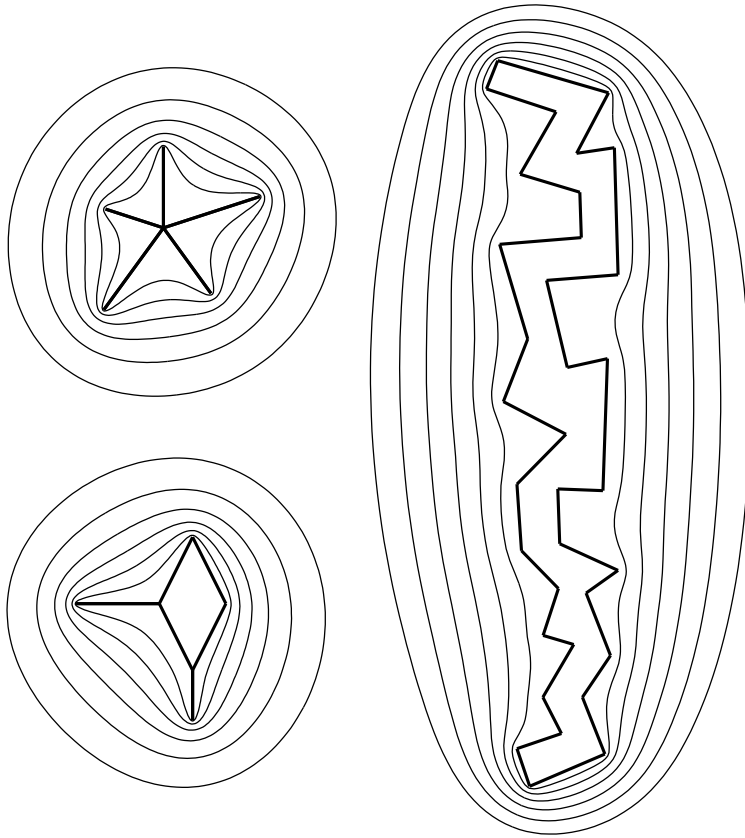


Figure 4.11. More examples of exterior SC maps. The radii of the circles are $0.4, \dots, 0.9$ on the left, and $0.7, 0.75, \dots, 0.95$ on the right.

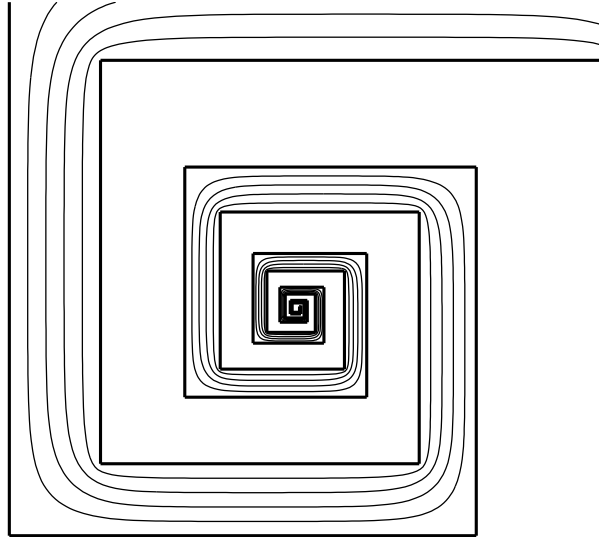


Figure 4.13. Map to a self-similar doubly infinite spiral with similarity factor $\gamma \approx 1.26$. In principle this SC map is completely described by just two unknowns. (The map is approximated here by truncation of an infinite product.)

$z_B - z_A$ and the real offset between prevertices on the top and bottom of S . These values are determined by two geometric conditions on $f(S)$: the length ratio of successive sides and the width of one “leg” of the spiral. This is a simple parameter problem. The infinite product in the SC integrand can again be truncated with little error. More complicated fractals (e.g., the exterior of the Koch snowflake) ought to be treatable using similar ideas, in a manner related to multipole methods [GR88]; some steps in this direction have been taken by Banjai [Ban00]. As a practical matter, however, one may get good results by truncating the fractal at a finite level of refinement and applying standard SC maps. See [BP93] for an example in the study of drag in fractally bounded channels.

plane.

The argument principle implies that f' must have b zeros in the upper half-plane H^+ . These points s_1, \dots, s_b are the preimages of the branch points. We therefore introduce the factors $(z - s_k)$ to f' . To keep them from affecting $\arg f'$ on the real axis, we also must multiply by $(z - \bar{s}_k)$. The map from H^+ to a Riemann surface is thus

Schwarz–Christoffel formula for Riemann surfaces

$$f(z) = A + C \int^z \prod_{k=1}^b (\zeta - s_k)(\zeta - \bar{s}_k) \prod_{k=1}^{n-1} (\zeta - z_k)^{\alpha_k - 1} d\zeta \quad (4.10)$$

Because Möbius transformations map inverse points to inverse points, the disk formula can be written as

$$f(z) = A + C \int^z \prod_{k=1}^b (\zeta - s_k)(1 - \bar{\zeta}\bar{s}_k) \prod_{k=1}^n \left(1 - \frac{\zeta}{z_k}\right)^{\alpha_k - 1} d\zeta, \quad (4.11)$$

where s_1, \dots, s_b are in the unit disk.

The extra $2b$ real unknowns (the roots of f') are determined by requiring that $f(s_k) = \sigma_k$ for $k = 1, \dots, b$. These unknowns can be transformed to incorporate their natural constraints implicitly. Overall the solution methodology is a fairly minor modification of the usual SC problem. Figure 4.17 illustrates a map to a Riemann surface.

Even though the map to a fully specified, polygonally bounded Riemann surface is readily computed, the reader is urged to think twice before pursuing this technique for an application. In some applications (see sections 5.3 and 5.4), Riemann surfaces arise naturally, but the geometry is discovered, not specified in advance; in other cases (such as the situation discussed in section 5.6 and [ET86]), they arise in some formulations of a problem but can be avoided by more careful ones.

4.8 Gearlike regions

A **gearlike region** is a Jordan region whose boundary segments are all either arcs of circles centered at the origin or segments of rays emanating from the origin. See Figure 4.18. The interior angles of such a region are integer multiples of $\pi/2$. The SC map to such regions was originally described by Goodman [Goo60] (who seems to have first applied the term *gear* in this context) and later by Mason and Jackson [JM87] and

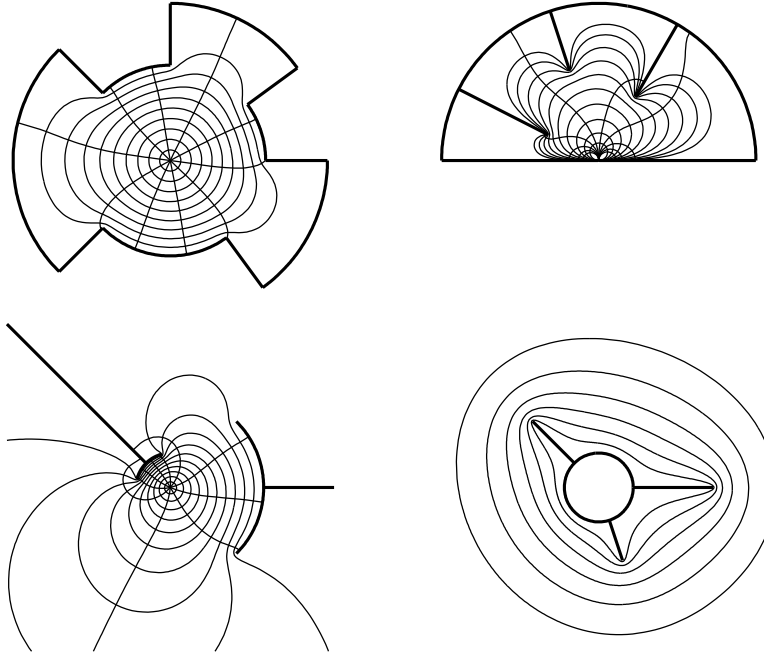


Figure 4.18. Maps to gearlike regions. At the upper right the map is from the half-plane; in the other cases, it is from the disk.

by Pearce [Pea91] (who implemented it numerically).

Figure 4.19 shows the logarithms of the regions of Figure 4.18. Each is a Riemann surface whose boundary is made up of horizontal and vertical line segments. One sheet of each surface is shown; dashed lines are to be identified. Notice that the appropriate condition on the interior angles is

$$\sum_{k=1}^n (\alpha_k - 1) = 0,$$

which corresponds to zero total turn. If the origin is on the boundary of P (as in the upper right of Figure 4.18), only one sheet is needed, and an ordinary SC map to $\log P$ is possible.

To proceed in the general case, we note that the map $\log(f(z))$ from the disk to $\log P$ should have the usual SC boundary behavior. However, if we evaluate this map around a loop enclosing the origin, we

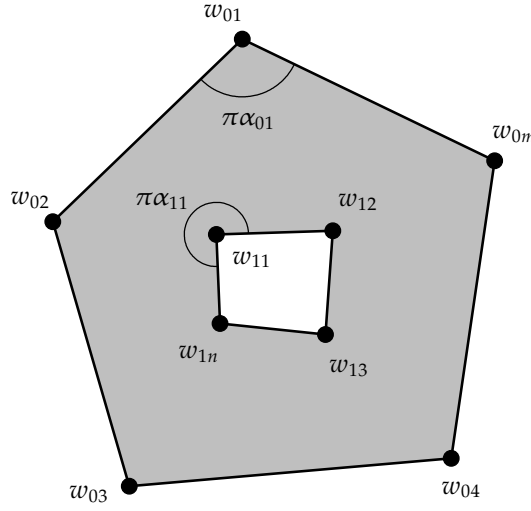


Figure 4.20. Notation for the doubly connected map.

not have a free multiplicative constant, we may not rescale the SC image. Moreover, the periodicity of $\log P$ is an additional constraint beyond the $n - 2$ side lengths that determine a regular polygon (see Theorem 3.1). Therefore, $n - 1$ side length conditions are needed to specify $\log P$ correctly.

The map to gearlike regions was described fully by Pearce [Pea91], who also made his software available (see section 3.6).

4.9 Doubly connected regions

The SC formula can be extended to doubly connected regions. Suppose P is bounded by an outer polygon, ∂_0 , and an inner polygon, ∂_1 . The vertices and interior angle parameters of ∂_0 are denoted by w_{01}, \dots, w_{0m} and $\alpha_{01}, \dots, \alpha_{0m}$; some of the w_{0k} may be infinite and thus $2 \leq \alpha_{0k} \leq 2$ as with the simply connected case. The inner boundary ∂_1 has n vertices, w_{11}, \dots, w_{1n} , which we require to be finite.⁵ The angle parameters of ∂_1 are measured in the interior of P and satisfy $0 < \alpha_{1k} \leq 2$. See Figure 4.20. From these definitions it is clear that

⁵ The 0 and 1 subscripts are conveniently reminiscent of “outer” and “inner.”

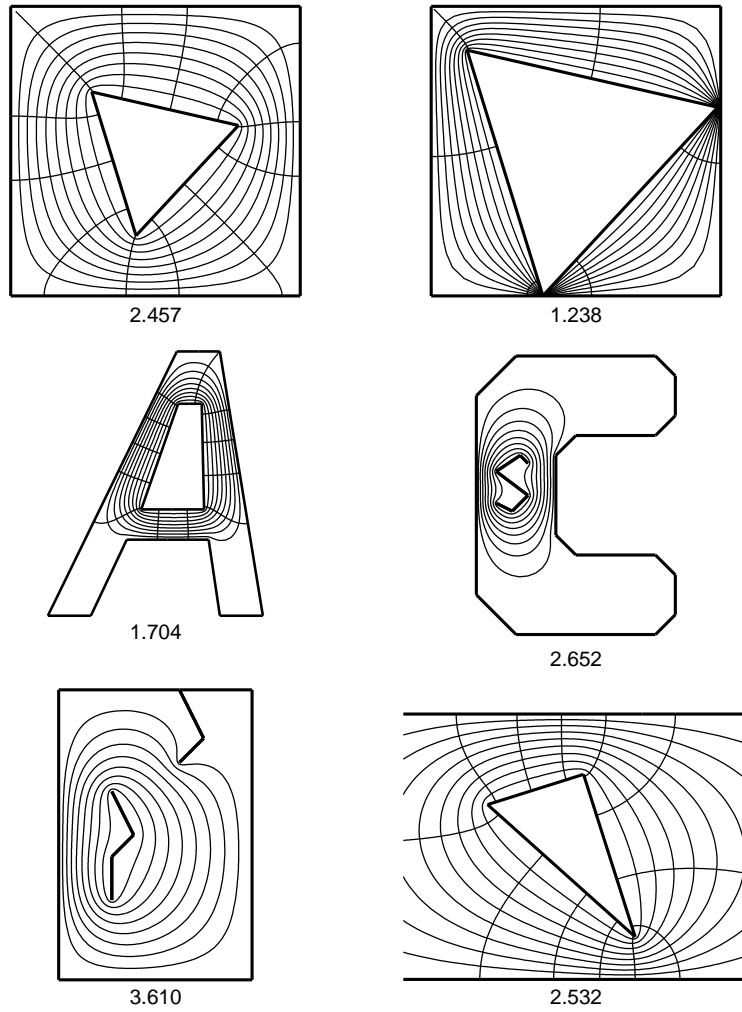


Figure 4.23. Examples of doubly connected SC maps. Underneath each map is shown the conformal modulus, μ^{-1} . These were computed using Hu's DSC-PACK.

CHAPTER 5

Applications

Conformal mapping in general, and Schwarz–Christoffel mapping in particular, are fascinating and beautiful subjects in their own rights. Nevertheless, the history of conformal mapping is driven largely by applications, so it is appropriate to consider when and how SC mapping can be used in practical problems.

It is not our intent in this final chapter to recount every instance in which Schwarz–Christoffel mapping has been brought to bear. Rather, after a brief look at a few areas full of such examples, we describe some situations in which SC ideas can be applied in ways that are computational and perhaps not transparent. The most famous application of conformal mapping is to Laplace’s equation, and we devote three sections to it. Beyond this it is clear that Schwarz–Christoffel mapping has a small but important niche in applied mathematics and science.

In applications it is common to pose a physical problem in the z -plane, which maps to a canonical region in the w -plane. This convention runs counter to our discussion in the earlier chapters, in which w was the plane of the polygon. In the following sections we attempt to be consistent with established applications literature where appropriate.

monic in H^+ , such that

$$\phi(x) = \begin{cases} \phi_1, & \infty < x < x_1 \\ \phi_2, & x_1 < x < x_2 \\ \vdots & \\ \phi_{\kappa-1}, & x_{\kappa-2} < x < x_{\kappa-1} \\ \phi_{\kappa}, & x_{\kappa-1} < x < \infty, \end{cases} \quad (5.2)$$

The solution of this boundary value problem is

$$\begin{aligned} \phi(z) = \operatorname{Re} \left[\frac{i}{\pi} \left(\phi_1 \log(z - x_1) + \phi_2 \log\left(\frac{z - x_2}{z - x_1}\right) \right. \right. \\ \left. \left. + \cdots + \phi_{\kappa-1} \log\left(\frac{z - x_{\kappa-1}}{z - x_{\kappa-2}}\right) - \phi_{\kappa} \log(x_{\kappa-1} - z) \right) \right]. \end{aligned} \quad (5.3)$$

(Caution is needed with branch cuts; it may be more convenient in computation to use $+\phi_{\kappa} \log[1/(x_{\kappa-1} - z)]$ in place of the last term in (5.3).) It is easy to verify that ϕ satisfies the stated boundary conditions. Figure 5.2 illustrates a solution obtained by this formula.

We have found $\phi(z)$ as the real part of an analytic map $f(z)$. Differentiating, we obtain

$$\begin{aligned} \frac{df}{dz} &= \frac{i}{\pi} \left[\frac{\phi_1}{z - x_1} + \frac{\phi_2(x_2 - x_1)}{(z - x_1)(z - x_2)} + \cdots - \frac{\phi_{\kappa}}{z - x_{\kappa-1}} \right] \\ &= i \frac{p(z)}{(z - x_1)(z - x_2) \cdots (z - x_{\kappa-1})}, \end{aligned} \quad (5.4)$$

where $p(z)$ is a real polynomial of degree at most $\kappa - 2$. Clearly, f is a Schwarz–Christoffel map! We summarize this observation as follows.

Theorem 5.1. *Given $m > 1$, real values $\phi_1, \dots, \phi_{\kappa}$, and $\infty < x_1 < x_2 < \cdots < x_{\kappa-1} < \infty$, there exists a unique real polynomial p of degree at most $\kappa - 2$ such that*

$$\phi(z) = \phi_1 + \operatorname{Re} \left[i \int_{x_1}^z p(\zeta) \prod_{k=1}^{\kappa-1} (\zeta - x_k)^{-1} d\zeta \right] \quad (5.5)$$

is the unique harmonic function in H^+ satisfying (5.2).

An examination of (5.4) reveals that if x_j is a root of $p(z)$, then $\phi_j = \phi_{j+1}$. In other words, a common factor in the fraction of (5.4) occurs if

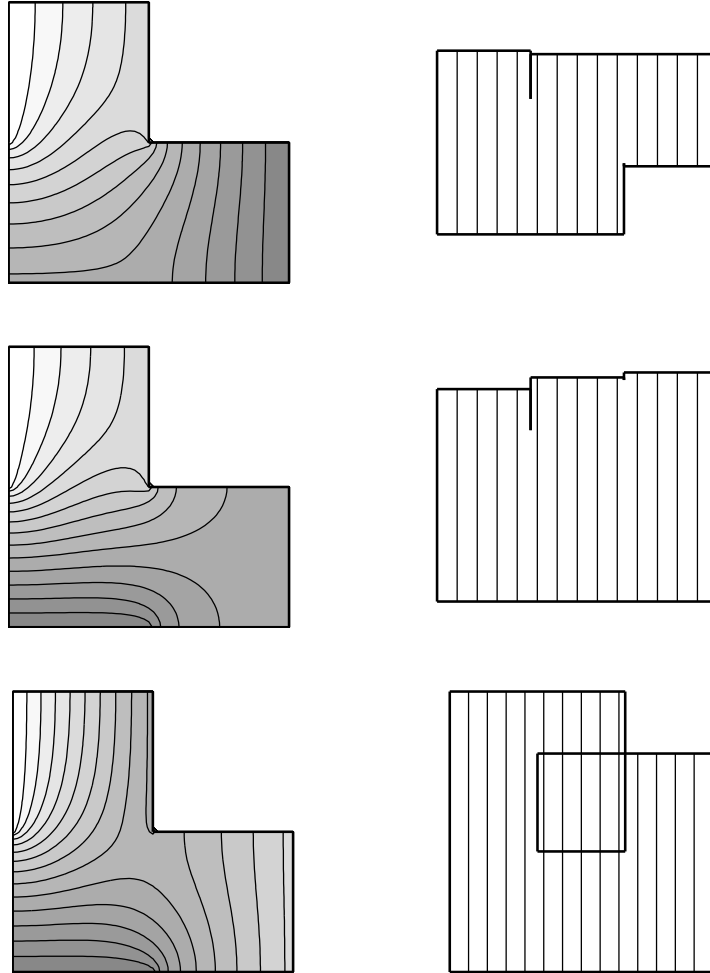


Figure 5.8. Examples of alternating D/N solutions on an L-shaped region. Every problem domain on the left has the same pattern of Dirichlet and Neumann assignments, and the same four Dirichlet values 1, 2, 3, 4, but the order of these values is different in each case. The right column shows the target regions obtained from Theorem 5.2; the solutions are the real parts of these maps. Level curves of each solution are drawn, and on the left these are shaded from 1 (white) to 4 (medium gray).

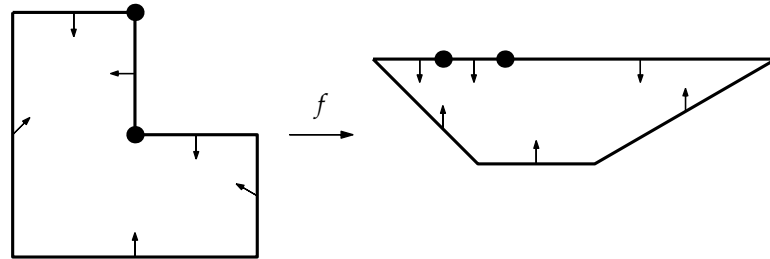


Figure 5.10. An oblique derivative problem on an L-shaped region and a map that suggests a solution.

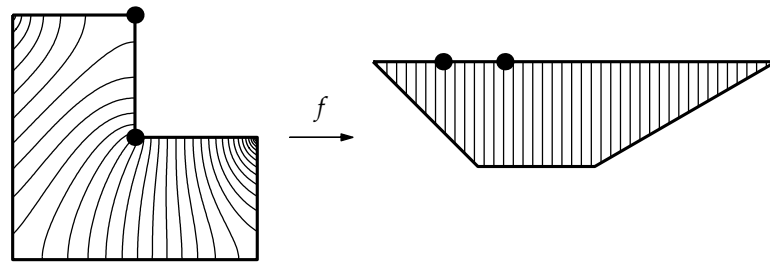


Figure 5.11. Solution of the L-shaped oblique derivative problem of Figure 5.10.

boundary condition does not change at these corners of P .

The discovered geometry of the image Q reveals information about the original problem. For example, in the present case, if $\phi = 0$ at the upper-left corner of P and $\phi = 1$ at the upper-right corner, we may compute from the position of the vertices along the boundary of Q that the values of ϕ at the six corners of P , beginning with the upper-left and proceeding counterclockwise, are 0, 0.2599, 0.5498, 1, 0.3267, and 0.1734. The reader who counts contours will note that eight or nine curves in the rightmost upper vertex of the L are so small as to be hidden under the thick line for the boundary; something like a fifth of the total “voltage drop” occurs in this millimeter or so of our figure.

Since all the boundary conditions of this problem are homogeneous, the solution is determined only up to a scale factor. We could multiply

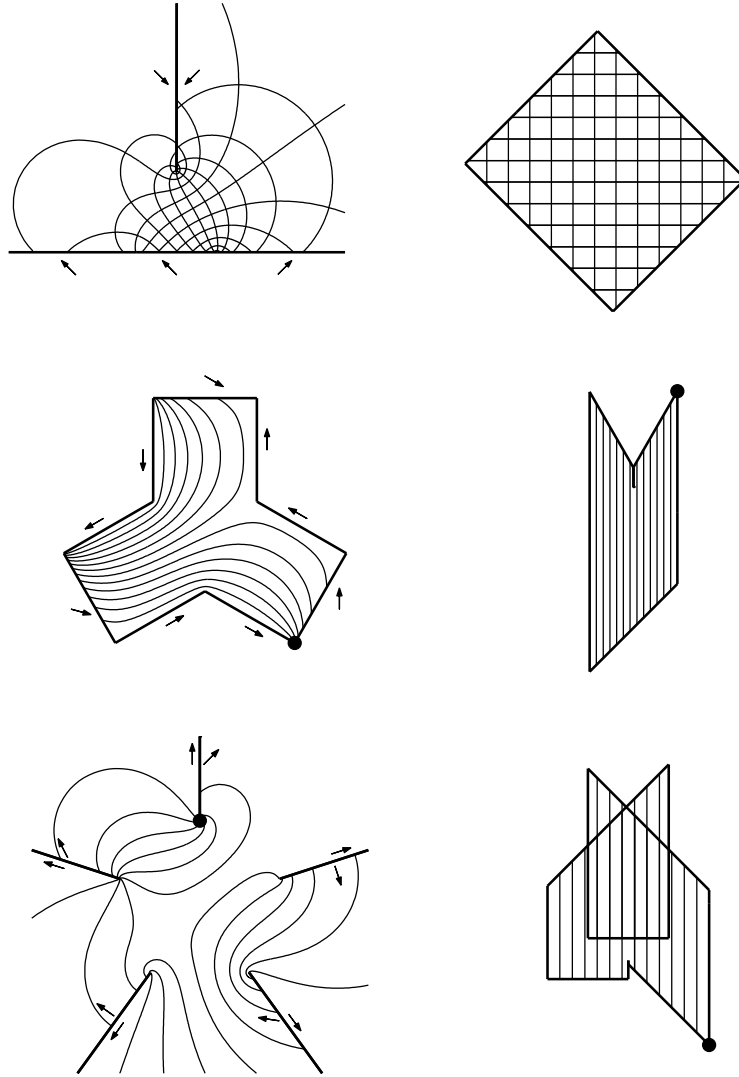


Figure 5.14. Examples of bounded solutions to oblique derivative problems of indices $\kappa = 2, 3, 4$ (top to bottom) on various domains. The arrows indicate the directions of zero derivative. Equipotentials (and, in the top case, flow lines) are shown.

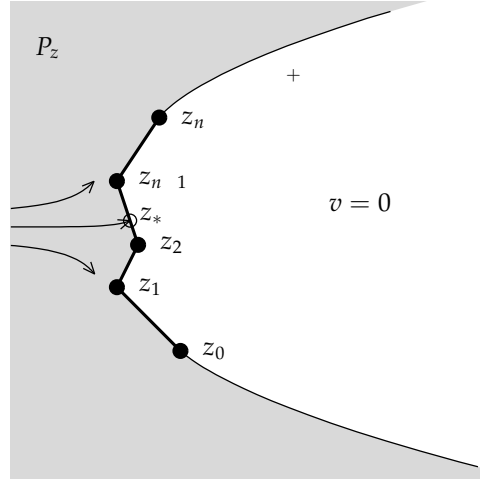


Figure 5.19. Wake flow past a polygonal obstacle.

passes the ends z_0 and z_n , it does not remain attached to the other side of the obstacle (that would require infinite acceleration); rather, it flows around a **wake** in which the (complex) fluid velocity $v(z)$ is zero. The curves $+$ and $-$ separating the wake from moving fluid are unknown free streamlines determined by $|v(z)| = 1$, a condition deriving from the continuity of pressure.

Let P_z be the region of moving fluid. Because the flow is incompressible and irrotational in P_z , v can be interpreted as the gradient of a real, harmonic potential. In complex terms we can write

$$\bar{v}(z) = \frac{dw}{dz} \quad (5.12)$$

for a new complex variable $w(z)$. The quantity \bar{v} is called the **hodo-graph** variable and is often given the symbol ζ . In the w -plane the obstacle is mapped to a slit, with the stagnation point mapping to the tip of the slit. See Figure 5.20. Without loss of generality, we assume that $w_* = w(z_*) = 0$. We make one further transformation that maps the slit plane P_w into the upper half-plane. This new variable x is given by

$$w = \frac{1}{2}W(x - x_*)^2, \quad (5.13)$$

where W and x_* are real constants chosen so that $x_0 = x(z_0) = -1$ and

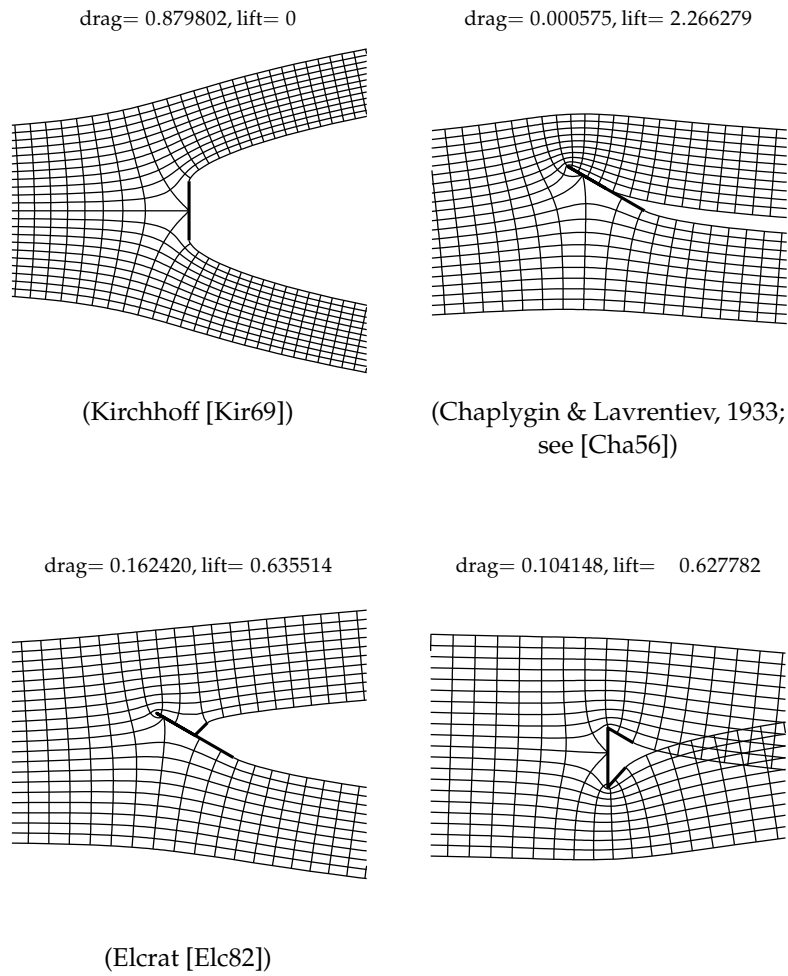


Figure 5.22. Examples of wake flows (data produced by program KIRCH1). At top left, the drag is known to be exactly $2\pi(4 + \pi) = 0.87980169\dots$. At top right, the separation point is specified on the middle of the plate; at bottom left, it is at the tip of the spoiler. At bottom right, the flow nonphysically crosses itself.

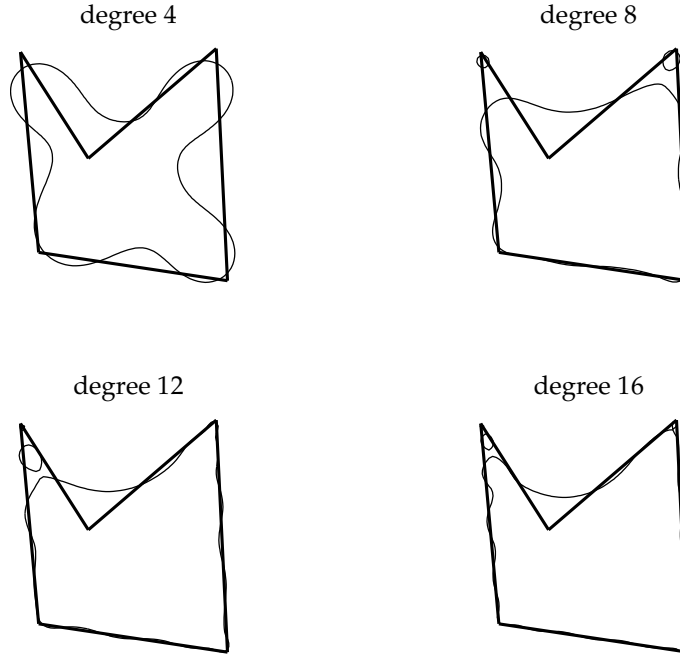


Figure 5.24. Level curves $|\phi_m| = 1$ of Faber polynomials. Because $\phi_m \approx \Phi^m$, the curves approximate the polygon. The re-entrant corner (with respect to the interior) is the last to be resolved.

imax problems. If the spectrum is well approximated by D , then the preceding map Φ leads to an estimate of the convergence rate of the Krylov method. Specifically, if $0 \notin D$ (the system is nonsingular), then

$$\lim_{m \rightarrow \infty} \|b - Ax_m\|^{1/m} \approx \frac{1}{|\Phi(0)|}. \quad (5.25)$$

Furthermore, the Faber polynomials can be used to construct the polynomials p_m of the Krylov method, given an estimate of the spectrum [SV93]. A similar approach using SCPACK was presented in [Li92]. For more about the connections between matrix iterations and complex approximation, see [DTT98, Gre96, Nev93]. In particular, [DTT98] discusses six factors that affect the quality of approximation in (5.25). Examples of the use of SC maps to construct and analyze matrix iterations

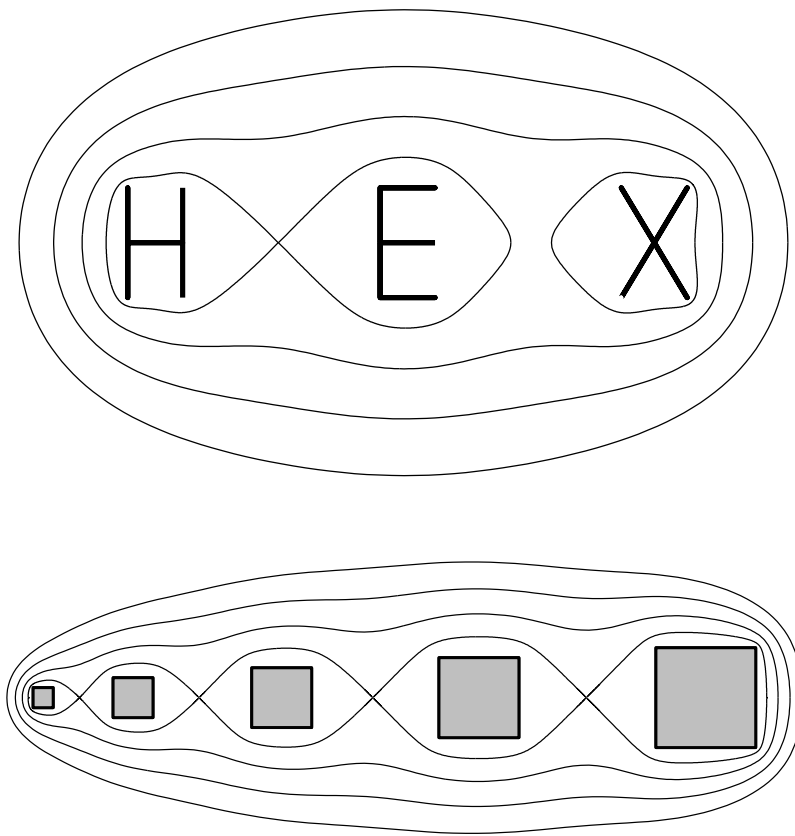


Figure 5.26. Examples of Green's functions for domains of connectivity three and five. Level curves are shown for each region. In the bottom picture, the gaps between squares were determined by solving a generalized parameter problem in order to make the four self-intersections occur.

APPENDIX

Using the SC Toolbox

Most of the figures in this book were produced using the SC Toolbox for MATLAB.¹ This software is in the public domain and is available (at the time of this writing) from

<http://www.math.udel.edu/~driscoll/SC/>

The toolbox is capable of half-plane and disk maps, exterior maps (section 4.4), strip maps (section 4.2), rectangle maps (section 4.3), and disk maps using the cross-ratio formulation (section 3.4). By tinkering with the provided routines, it is not too hard to produce maps to gearlike regions (section 4.8) and Riemann surfaces (section 4.7). Other variations and applications require more extensive programming efforts.

The toolbox defines polygons and the maps to them as named objects. Once created, these objects can be manipulated by using common MATLAB functions and notations that have been extended to understand them. The main examples are

¹ Version 2.1 of the SC Toolbox and versions 5.2–6.0 of MATLAB. The first author hopes to maintain compatibility with future versions of MATLAB indefinitely. MATLAB is a registered trademark of The Mathworks, Inc., which has no affiliation with or responsibility for the SC Toolbox.


```

p = polygon([i,-i,Inf],[3/2,1/2,-1]);
f = hplmap(p);
axis([-3 3 -1.5 4.5]), hold on
plot(f,0.7*(-10:6),0.7*(1:12))

```

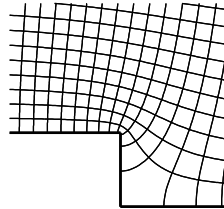


(Figure 2.10)

```

p = polygon([-4-i,4-i,4+i,-4+i]);
f = diskmap(p);
f = center(f,0);
plot(f,0.2*(1:4),angle(prevertex(f)))

```

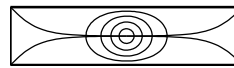


(Figure 2.13)

```

w = [Inf,-1-i,-2.5-i,Inf,2.4-3.3i,...
      Inf,2.4-1.3i,Inf,-1+i,-2.5+i];
alf = [0,2,1,-.85,2,0,2,-1.15,2,1];
p = polygon(w,alf);
f1 = stripmap(p,[6 8]);
f2 = stripmap(p,[4 8]);
axis([-4.3 5.7 -6.15 3.85]), hold on
plot(f1,0,8)
pause, cla
plot(f2,0,8)

```

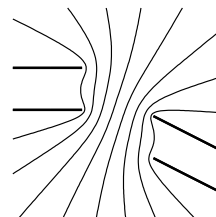
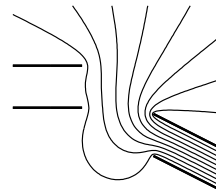


(Figure 4.6)

```

p = polygon([-5-i,-5-3i,5-3i,...
      5+i,5+3i,-5+3i]);
f = rectmap(p,[1 2 4 5]);
plot(f)

```

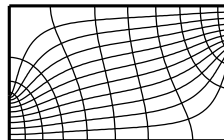


(Figure 4.8)

Bibliography

- [ADHE82] O. L. Anderson, R. T. Davis, G. B. Hankins, and D. E. Edwards. Solution of viscous internal flows on curvilinear grids generated by the Schwarz–Christoffel transformation. *Appl. Math. Comput.*, 10:507–24, 1982.
- [AF97] M. J. Ablowitz and A. S. Fokas. *Complex Variables: Introduction and Applications*. Cambridge University Press, New York, 1997.
- [Ahl78] L. V. Ahlfors. *Complex Analysis*. McGraw–Hill, New York, 3rd edition, 1978. An introduction to the theory of analytic functions of one complex variable.
- [Akh56] N. Akhiezer. *Theory of Approximation*. Ungar, New York, 1956.
- [And75] R. Anderson. Analogue-numerical approach to conformal mapping. *Proc. IEE*, 122:874–76, 1975.
- [Ban00] L. Banjai. Recursive algorithms in complex analysis. Unpublished honors project in Mathematics and Computation, Oxford University, 2000.
- [BE92] M. Bern and D. Eppstein. Mesh generation and optimal triangulation. In D. Z. Du and F. Hwang, editors, *Computing in Euclidean Geometry*. World Scientific, 1992. Also Xerox Palo Alto Research Center Technical report CSL-92-1.

- [vS59] W. von Koppenfels and R. W. Stallman. *Praxis der Konformen Abbildung*. Springer, Berlin, 1959.
- [VT73] V. V. Vecheslavov and N. I. Tolstobrova. Parameters for the conformal mapping of symmetric doubly connected polygonal regions (English translation). *USSR Comput. Math. Math. Phys.*, 13:49–57, 1973.
- [Wal64] M. Walker. *The Schwarz–Christoffel Transformation and Its Applications—A Simple Exposition*. Dover, New York, 1964. First published in 1933 by Oxford University under the title, *Conjugate Functions for Engineers*.
- [Weg86] R. Wegmann. An iterative method for conformal mapping. *J. Comp. Appl. Math.*, 14:7–18, 1986.
- [Wen82] M. Wenocur. *A Production Network Model and its Diffusion Approximation*. Phd thesis, Department of Statistics, Stanford University, 1982.
- [Wic54] R. F. Wick. Solution of the field problem of the Germanium gyrator. *J. Appl. Phys.*, 25:741–56, 1954.
- [Wid69] H. Widom. Extremal polynomials associated with a system of curves in the complex plane. *Adv. Math.*, 3:127–232, 1969.
- [Wil95] R. J. Williams. Semimartingale reflecting Brownian motions in the orthant. In *Stochastic Networks*, pages 125–37. Springer, New York, 1995.
- [Woo61] L. C. Woods. *The Theory of Subsonic Plane Flow*. Cambridge University Press, 1961.